# Chapter 6
# Multiphase Flow

**Yonghui Huang and Haibing Shao**

In this chapter, we consider two-phase two-component transport process with phase transition phenomenon.

## 6.1 Gas Injection and Migration in Fully Water Saturated Column

The background of this benchmark is the production of hydrogen gas due to the corrosion of the metallic container in the nuclear waste repository. Numerical model is built to illustrate such gas appearance phenomenon. The model domain is a two dimensional horizontal column representing the bentonite backfill in the repository tunnel, with hydrogen gas injected on the left boundary. This benchmark was proposed in the GNR MoMaS project by French National Radioactive Waste Management Agency. Several research groups has made contributions to test the benchmark and provided their reference solutions Ben Gharbia and Jaffré (2014), Bourgeat et al. (2009), Marchand and Knabner (2014b), Neumann et al. (2013). Here we adopted the results proposed in Marchand and Knabner (2014b) for comparison.

Y. Huang (✉)
UFZ, Helmholtz Centre for Environmental Research, Leipzig, Germany
e-mail: yonghui.huang@ufz.de

H.B. Shao
Department Environmental Informatics, Helmholtz Centre for Environmental Research—UFZ, Leipzig, Germany



O. Kolditz et al. (eds.), *Thermo-Hydro-Mechanical-Chemical Processes in Fractured Porous Media: Modelling and Benchmarking*, Terrestrial Environmental Sciences, DOI 10.1007/978-3-319-29224-3_6

### 6.1.1 Physical Scenario

Here a 2D rectangular domain $\Omega = [0, 200] \times [-10, 10]$ m (see Fig. 6.1) was considered with an impervious boundary at $\Gamma_{imp} = [0, 200] \times [-10, 10]$ m, an inflow boundary at $\Gamma_{in} = \{0\} \times [-10, 10]$ m and an outflow boundary at $\Gamma_{out} = \{200\} \times [-10, 10]$ m. The domain was initially saturated with water, hydrogen gas was injected on the left-hand-side boundary within a certain time span ($[0, 5 \times 10^4$century]). After that the hydrogen injection stopped and no flux came into the system. The right-hand-side boundary is kept open throughout the simulation. The initial condition and boundary conditions were summarized as

- $X(t = 0) = 10^{-5}$ and $P_L(t = 0) = P_L^{out} = 10^6$ [Pa] on $\Omega$.
- $q^w \cdot \nu = q^h \cdot \nu = 0$ on $\Gamma_{imp}$.
- $q^w \cdot \nu = 0, q^h \cdot \nu = Q_d^h = 0.2785$ [mol century$^{-1}$m$^{-2}$] on $\Gamma_{in}$.
- $X = 0$ and $P_l = P_L^{out} = 10^6$ [Pa] on $\Gamma_{out}$.

### 6.1.2 Model Parameters and Numerical Settings

The capillary pressure $P_c$ and relative permeability functions are given by the van-Genuchten model (Van Genuchten 1980).

$$P_c = P_r \left( S_{le}^{-\frac{1}{m}} - 1 \right)^{\frac{1}{n}}$$

$$K_{r_L} = \sqrt{S_{le}} \left( 1 - \left( 1 - S_{le}^{\frac{1}{m}} \right)^m \right)^2$$

$$K_{r_G} = \sqrt{1 - S_{le}} \left( 1 - S_{le}^{\frac{1}{m}} \right)^{2m}$$

where $m = 1 - \frac{1}{n}$, $P_r$ and $n$ are van-Genuchten model parameters and the effective saturation $S_{le}$ is given by

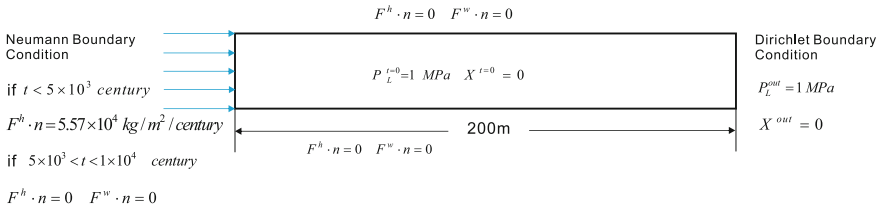


**Fig. 6.1** Geometry and boundary condition for the $H_2$ injection benchmark

**Table 6.1** Fluid and porous medium properties applied in the $H_2$ migration benchmark

| Parameters | Symbol | Value | Unit |
|---|---|---|---|
| Intrinsic permeability | $K$ | $5 \times 10^{-20}$ | [$m^2$] |
| Porosity | $\Phi$ | 0.15 | – |
| Residual saturation of liquid phase | $S_{lr}$ | 0.4 | [–] |
| Residual saturation of gas phase | $S_{gr}$ | 0 | [–] |
| Viscosity of liquid | $\mu_l$ | $10^{-3}$ | [Pa · s] |
| Viscosity of gas | $\mu_g$ | $9 \times 10^{-6}$ | [Pa · s] |
| van Genuchten parameter | $P_r$ | $2 \times 10^6$ | [Pa] |
| van Genuchten parameter | $n$ | 1.49 | – |

$$S_{le} = \frac{1 - S_g - S_{lr}}{1 - S_{lr} - S_{gr}} \tag{6.1.1}$$

here $S_{lr}$ and $S_{gr}$ indicate the residual saturation in liquid and gas phases, respectively. Values of parameters applied in this model are summarized in Table 6.1.

We created a 2D triangular mesh here with 963 nodes and 1758 elements. The mesh element size varies between 1 and 5 m. A fixed time step size of 1 century is applied. The entire simulated time from 0 to $10^4$ centuries were simulated. The entire execution time is around $3.241 \times 10^4$s.

### *6.1.3 Results and Analysis*

The results of this benchmark are depicted in Fig. 6.2. The evolution of gas phase saturation and the gas/liquid phase pressure over the entire time span are shown. In additional, we compare results from our model against those given in Marchand and Knabner (2014b). In Fig. 6.2, solid lines are our simulation results while the symbols are the results from Marchand et al. It can be seen that a good agreement has been achieved. Furthermore, the evolution profile of the gas phase saturation $S_g$, the liquid phase pressure $P_L$, and the total molar fraction of hydrogen $X$ are plotted at different time ($t = 150, 1 \times 10^3, 5 \times 10^3, 6 \times 10^3$ centuries) in Fig. 6.3a–c respectively.

By observing the simulated saturation and pressure profile, the complete physical process of $H_2$ injection can be categorized into five subsequent stages.

**(1) The dissolution stage**: After the injection of hydrogen at the inflow boundary, the gas first dissolved in the water. This was reflected by the increasing concentration of hydrogen in Fig. 6.3c. Meanwhile, the phase pressure did not vary much and was kept almost constant (see Fig. 6.3b).

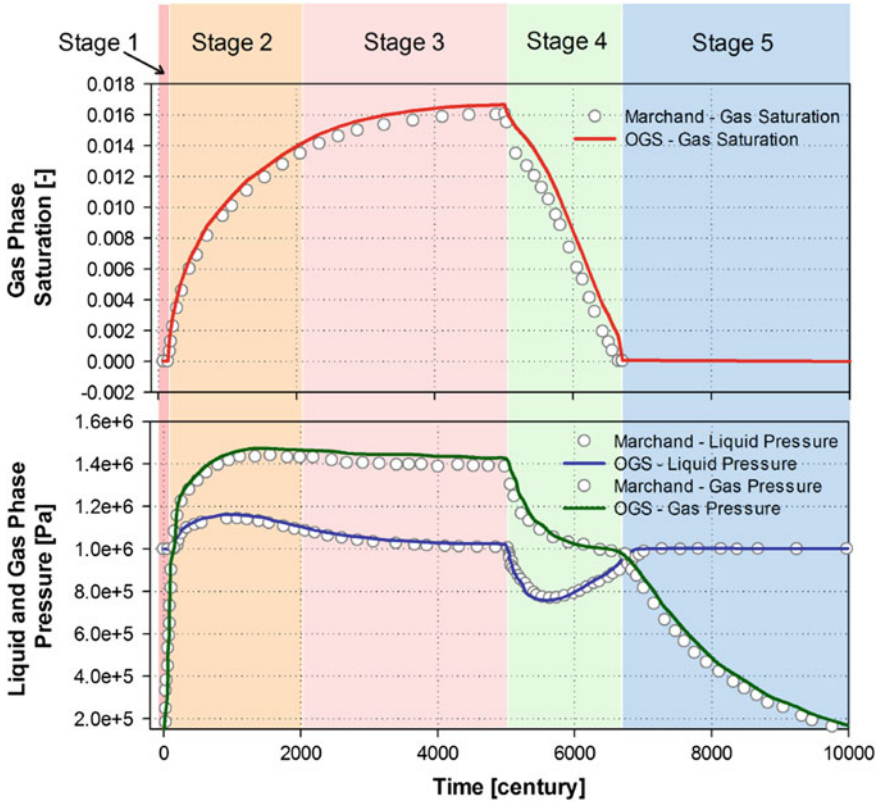


**Fig. 6.2** Evolution of pressure and saturation over time

**(2) Capillary stage**: Given a constant temperature, the maximal soluble amount of $H_2$ in the water liquid is a function of pressure. In this MoMaS benchmark case, our simulation showed that this threshold value was about $1 \times 10^{-3}$ mol $H_2$ per mol of water at a pressure of $1 \times 10^6$ [Pa]. Once this pressure was reached, the gas will emerge and formed a continuous phase. As shown in Fig. 6.3a, at approximately 150 centuries, the first phase transition happens. Beyond this point, the gas and liquid phase pressure quickly increase, while hydrogen gas is transported towards the right boundary driven by the pressure and concentration gradient. In the meantime, the location of this phase transition point also slowly shifted towards the middle of the domain.

**(3) Gas migration stage**: The hydrogen injection process continued until the 5000th century. Although the gas saturation continues to increase, pressures in both phases begin to decline due to the existence of the liquid phase gradient. Eventually, the whole system will reach steady state with no liquid phase gradient.

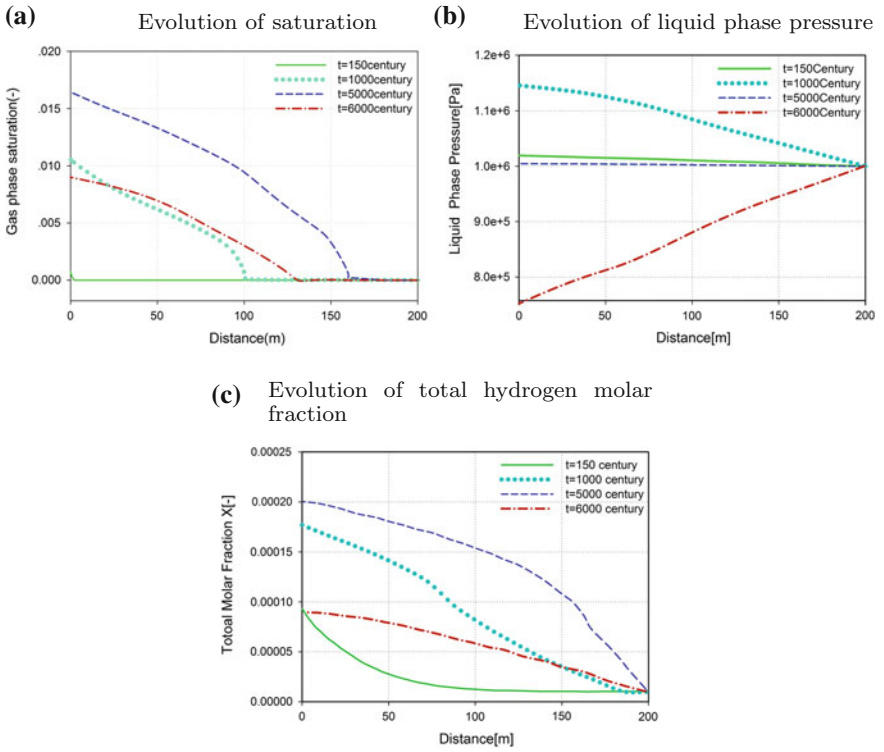


**Fig. 6.3** Evolution of **a** gas phase saturation **b** liquid phase pressure and **c** total hydrogen molar fraction over the whole domain at different time

**(4) Recovery stage**: After hydrogen injection was stopped at the 5000th century, the water came back from the outflow boundary towards the left, which was driven by the capillary effect to occupy the space left by the disappearing gas phase. During this stage, the gas phase saturation begins to decline, and both phase pressures drop even below the initial pressure. The whole process will not stop until the gas phase completely disappeared.

**(5) Equilibrium stage**: After the complete disappearance of the gas phase, the saturation comes to zero again, and the whole system will reach steady state, with pressure and saturation values same as the ones given in the initial condition.

## 6.2 MoMaS Benchmark 2: Gas Injection and Migration in Partially Water Saturated Column

The physical setting of this benchmark is very similar to the previous one. The only difference is the column is initially partially saturated with water, which indicates the gas exist at the beginning of the simulation.

### 6.2.1 Physical Scenario

The physical scenario of this benchmark is exactly the same as the first MoMaS benchmark. However, the initial and boundary condition will be altered, and the total simulation time will be different as well. The initial gas phase pressure was set to be $1.1e+6$ [Pa] which is bigger than the liquid phase pressure( $1.e+6$ [Pa]) to ensure the presence of gas phase in the whole domain, while on the inflow boundary $\Gamma_{in}$ the Dirichlet boundary was chosen the same as the initial condition in order to keep the presence of gas phase on the boundary. A constant hydrogen gas flux was imposed on the left-hand-side boundary. The initial condition and boundary conditions were summarized as:

- $X(t=0) = 0.018762136579995$ and $P_L(t=0) = P_L^{out} = 10^6$ [Pa] on $\Omega$.
- $q^w \cdot \nu = q^h \cdot \nu = 0$ on $\Gamma_{imp}$.
- $q^w \cdot \nu = 0, q^h \cdot \nu = Q_d^h = 2.785$ [mol century$^{-1}$m$^{-2}$] on $\Gamma_{in}$.
- $X = 0.018762136579995$ and $P_l = P_L^{out} = 10^6$ [Pa] on $\Gamma_{out}$.

The model parameters can be referred to Table 6.1.

### 6.2.2 Results and Analysis

The results of this benchmark are depicted in Figs. 6.4, 6.5 and 6.6. The evolution profile of the gas phase saturation $S_g$, the liquid phase pressure $P_L$, and the total molar fraction of hydrogen $X$ are plotted at different time respectively. We compare results from our model against those given in Bourgeat et al. (2013). In all these figures, solid lines are our simulation results while the symbols are the results from Bourgeat et al. It can be seen that a good agreement has been achieved.

By observing the simulated saturation and pressure profile, the complete physical process of $H_2$ injection can be categorized into four subsequent stages.

**(1)** up to t $<$ 1,400 years, the two phases are present in the whole domain (see time t $=$ 500 years in Fig. 6.4). The injection of hydrogen flux increases the gas saturation in the vicinity of inflow boundary $\Gamma_{in}$. The drop of gas saturation is due to the difference in relative mobilities between the two phases: the lower liquid mobility leads to a bigger liquid pressure accumulation, compared to the increase of the gas pressure, which is finally resulting in a decrease of capillary pressure and a liquid saturated zone is generated (see Fig. 6.5).

**(2)** At time t $=$ 1,400 years, the gas phase starts to disappear in some region of the porous domain (see time t $=$ 1,500 years, in Fig. 6.4a). Then, a fully saturated liquid region (Sg = 0) will exist until time t $=$ 17,000 years (see Fig. 6.4a), and during this period of time, the saturated region is pushed by the injected hydrogen, from $\Gamma_{in}$ to $\Gamma_{out}$.

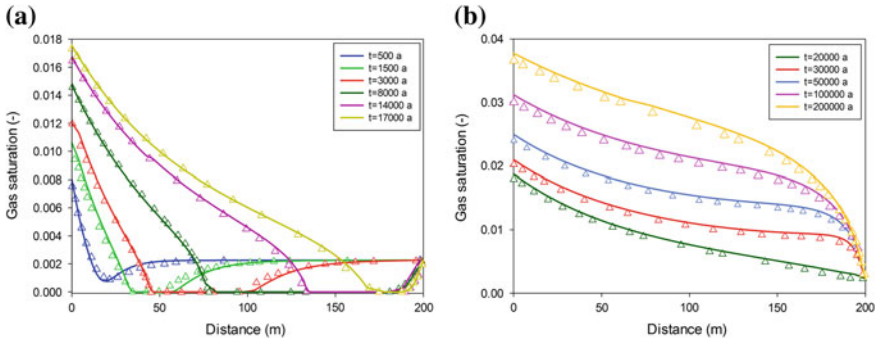


**Fig. 6.4** Evolution of gas phase saturation over the whole domain at different time

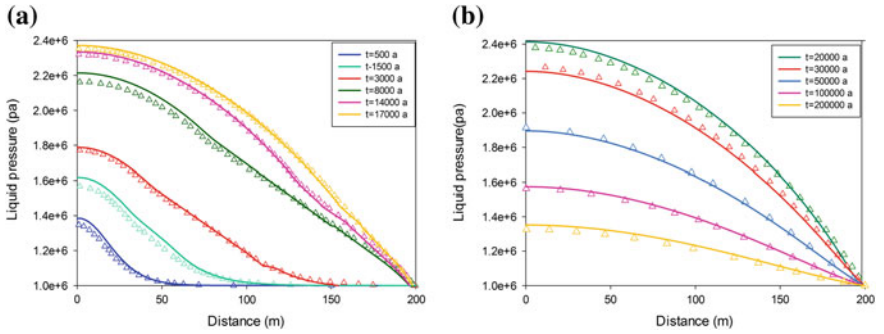


**Fig. 6.5** Evolution of liquid phase pressure over the whole domain at different time

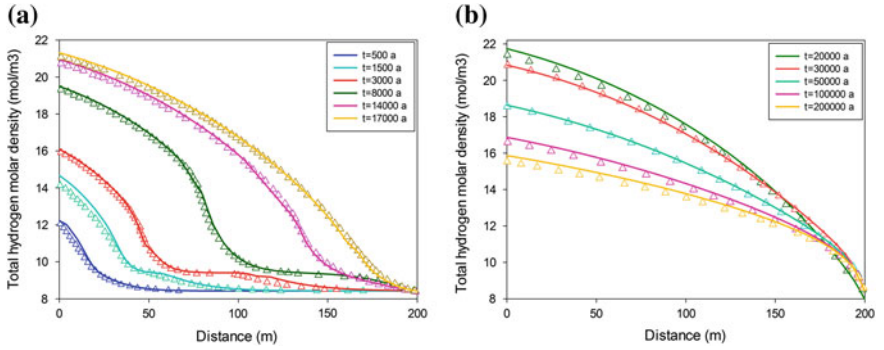


**Fig. 6.6** Evolution of total hydrogen molar density over the whole domain at different time

**(3)** After the time t = 17,000 years, due to the Dirichlet conditions imposed on $\Gamma_{out}$, the liquid saturated region disappears and all together the phases' pressure and the gas saturation are growing in the whole domain (see the time t = 20,000 years in Figs. 6.4b and 6.5b).

**(4)** Finally, the liquid pressure reaches its maximum at time t = 20,000 years and then decreases in the whole domain (see Fig. 6.5b). This is caused, like in the benchmark 1, by the evolution of the system towards a stationary state.

## 6.3 Heat Pipe Problem with Phase Appearance and Disappearance

The thermal effects on multiphase formulation with phase transition phenonmena are investigated. We adopted the heat pipe problem proposed by Udell and Fitch Udell and Fitch (1985). They have provided a semi-analytical solution for a non-isothermal water-gas system in porous media, where heat convection, heat conduction as well as capillary forces were considered. A heater installed on the right-hand-side of the domain generated constant flux of heat, and it was then transferred through the porous media by conduction, as well as the enthalpy transport of the fluids. The semi-analytical solution was developed for the steady state condition, and the liquid phase flowed in the opposite direction to the gas phase. If gravity was neglected, the system can be simplified to a system of six ordinary differential equations (ODE), the solution of which was then be obtained in the form of semi-analytical solution. Detailed derivation procedure is available in Helmig (1997), Huang et al. (2015b), and the parameters used in our comparison are listed in Table 6.2.

### *6.3.1 Physical Scenario*

As shown in Fig. 6.7, the heat pipe was represented by a 2D horizontally column (2.25 m in length and 0.2 m in diameter) of porous media, which was partially saturated with a liquid phase saturation value of 0.7 at the beginning. A constant heat flux ($Q_T = 100$ [W m$^{-2}$]) was imposed on the right-hand-side boundary $\Gamma_{in}$, representing the continuously operating heating element. At the left-hand-side boundary $\Gamma_{out}$, Dirichlet boundary conditions were imposed for Temperature $T = 70$°C, liquid phase pressure $P_G = 1 \times 10^5$ [Pa], effective liquid phase saturation $S_{le} = 1$, and air molar fraction in the gas phase $X_G^a = 0.71$. Detailed initial and boundary condition are summarized as follows.

- $P(t=0) = 1 \times 10^5$ [Pa], $S_L(t=0) = 0.7$, $T(t=0) = 70$ [°C] on the entire domain.
- $q^w \cdot \nu = q^h \cdot \nu = 0$ on $\Gamma_{imp}$.
- $q^w \cdot \nu = q^h \cdot \nu = 0$, $q^T \cdot \nu = Q_T$ on $\Gamma_{in}$.
- $P = 1 \times 10^5$ [Pa], $S_L = 0.7$, $T = 70$ [°C] on $\Gamma_{out}$.

**Table 6.2** Parameters applied in the Heat pipe problem

| Parameters name | Symbol | Value | Unit |
|---|---|---|---|
| Permeability | $K$ | $10^{-12}$ | [$m^2$] |
| Porosity | $\Phi$ | 0.4 | [–] |
| Residual liquid phase saturation | $S_{lr}$ | 0.4 | [–] |
| Heat conductivity of fully saturated porous medium | $\lambda_{pm}^{S_w=1}$ | 1.13 | [W $m^{-1}$ $K^{-1}$] |
| Heat conductivity of dry porous medium | $\lambda_{pm}^{S_w=0}$ | 0.582 | [W $m^{-1}$ $K^{-1}$] |
| Heat capacity of the soil grains | $c_s$ | 700 | [J $kg^{-1}$ $K^{-1}$] |
| Density of the soil grain | $\rho_s$ | 2600 | [kg $m^{-3}$] |
| Density of the water | $\rho_w$ | 1000 | [kg $m^{-3}$] |
| Density of the air | $\rho$ | 0.08 | [kg $m^{-3}$] |
| Dynamic viscosity of water | $\mu_w$ | $2.938 \times 10^{-4}$ | [Pa · s] |
| Dynamic viscosity of air | $\mu_g^a$ | $2.08 \times 10^{-5}$ | [Pa · s] |
| Dynamic viscosity of steam | $\mu_g^w$ | $1.20 \times 10^{-5}$ | [Pa · s] |
| Diffusion coefficient of air | $D_g^a$ | $2.6 \times 10^{-5}$ | [$m^2$ $s^{-1}$] |
| van Genuchten parameter | $P_r$ | $1 \times 10^4$ | [Pa] |
| van Genuchten parameter | $n$ | 5 | [−] |

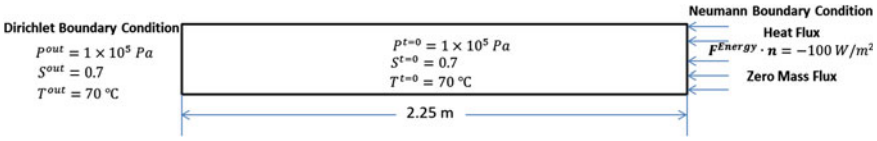


**Fig. 6.7** Geometry and boundary condition for the $H_2$ injection benchmark

## *6.3.2 Model Parameters and Numerical Settings*

For the capillary pressure-saturation relationship, van Genuchten model was applied. The parameters used in the van Genuchten model are listed in Table 6.2. The water-air relative permeability relationships were described by the Fatt and Klikoffv formulations Fatt et al. (1959).

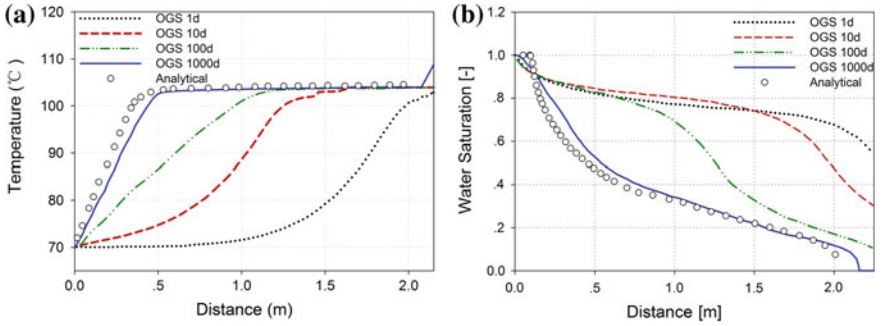


Evolution of Temperature Evolution of liquid phase saturation

**Fig. 6.8** Evolution of **a** temperature and **b** liquid phase saturation over the whole domain at different time

$$K_{rG} = (1 - S_{le})^3$$
$$K_{rL} = S_{le}^3$$

where $S_{le}$ is the effective liquid phase saturation, referred to Eq. (6.1.1).

We created a 2D triangular mesh here with 206 nodes and 326 elements. The averaged mesh element size is around 6 m. A fixed size time stepping scheme has been adopted, with a constant time step size of 0.01 day. The entire simulated time from 0 to $10^4$ day were simulated.

### *6.3.3 Results and Analysis*

The results of our simulation were plotted along the central horizontal profile over the model domain at y = 0.1 m, and compared against semi-analytical solution. Temperature and saturation profiles at day 1, 10, 100, 1000 are depicted in Fig. 6.8a, b respectively. As the heat flux was imposed on the right-hand-side boundary, the temperature kept rising there. After 1 day, the boundary temperature already exceeded 100 °C, and the water in the soil started to boil. Together with the appearance of steam, water saturation on the right-hand-side began to decrease. After 10 days, the boiling point has almost moved to the middle of the column. Meanwhile, the steam front kept boiling and shifted to the left-hand-side, whereas liquid water was drawn back to the right. After about 1000 days, the system reached a quasi-steady state, where the single phase gas, two phase and single phase liquid regions co-exist and can be distinguished. A pure gas phase region can be observed on the right and liquid phase region dominates the left side.